Supporting Information

Verbrugge et al. 10.1073/pnas.0905177106

SI Text

Estimate of the Limits on Deriving the Relative Distances from the FRET Efficiency. From the FRET efficiencies we obtained, donor–acceptor distances can only be estimated, because the relative orientations and orientational freedom of the fluorophores are not known. To obtain an estimate of the distances, we assumed that the fluorophores are free to rotate. Under these conditions, distances can be calculated using Förster's relation (1):

$$R = R_0 \sqrt[6]{\frac{1 - E_{FRET}}{E_{FRET}}} \quad \textbf{[S1]}$$

where R is the distance between donor and acceptor and R_0 is the Förster distance (5.1 nm for FRET between Alexa Fluor 555 and Alexa Fluor 647; Molecular Probes). Using this equation, we find that the donor–acceptor distance is ≈3.7 nm for a transfer efficiency of 0.88 (T324C) and ≈4.5 nm for a transfer efficiency of 0.69 (S43C).

1. Förster T (1948) Zwischenmolekulare energiewanderung und fluoreszenz. *Ann Physik* 437:55–75.

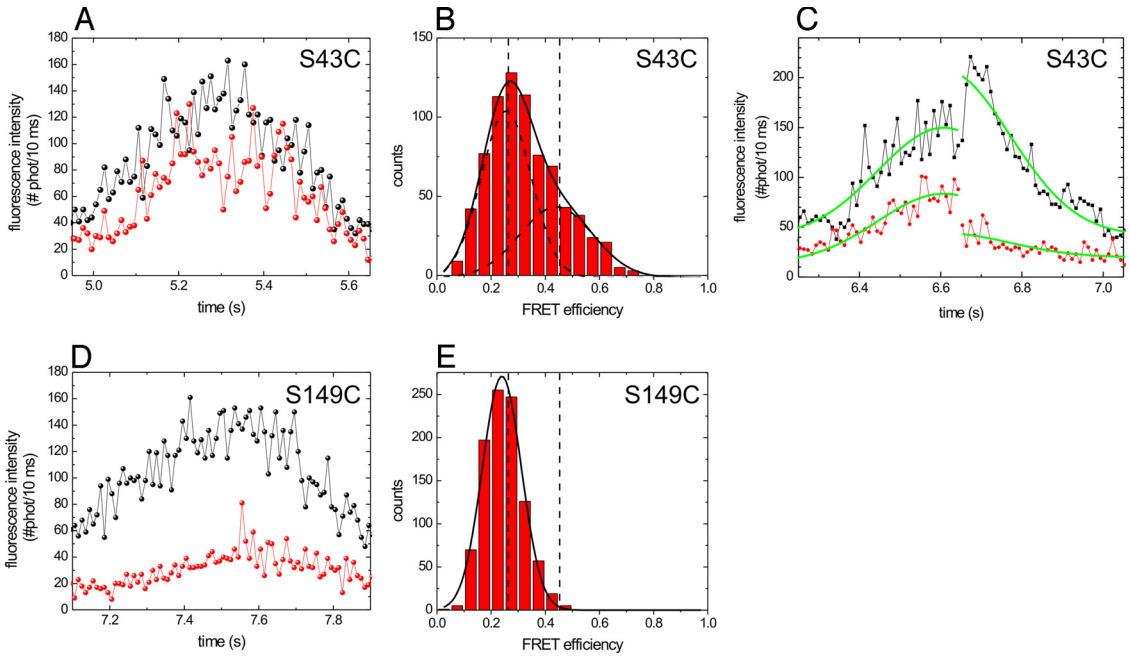

Fig. S1. Fluorescence intensity time traces and histograms of the apparent FRET efficiencies indicate that S43C shows FRET and S149C does not. ATP concentration: 2 mM. (*A*) Intensity time trace (number of photons per 10-ms bin) of an S43C kinesin with a donor and acceptor. Large intensity fluctuations (≈30%) can be discerned that appear anticorrelated in donor (black) and acceptor (red) traces. (*B*) Histogram of the apparent FRET efficiency [$I_a/(I_a + I_d)$ of eight events of the S43C construct, showing a peak at a FRET efficiency of 0.256 ± 0.012 and a second peak at 0.45 ± 0.09 (as obtained by fitting two Gaussians)]. The histogram was obtained from the central 200 ms of intensity time traces (2-ms binned). (*C*) Fluorescence intensity time trace of an S43C event where the acceptor photo bleached. After acceptor photo bleaching (at ≈6.65 s), the donor intensity increases by a factor of 1.5 ± 0.1. ATP concentration: 2 mM. (*D*) Intensity time trace of a single S149C donor–acceptor labeled kinesin. In this trace, the intensity fluctuations are substantially smaller than in *A*, in both donor (black) and acceptor channel (red). (*E*) Histogram of the apparent FRET efficiency of 6 events of S149C. This histogram shows only a single peak with a value of 0.240 ± 0.002 (from fitted Gaussian), corresponding to the low-FRET peak in *B*.

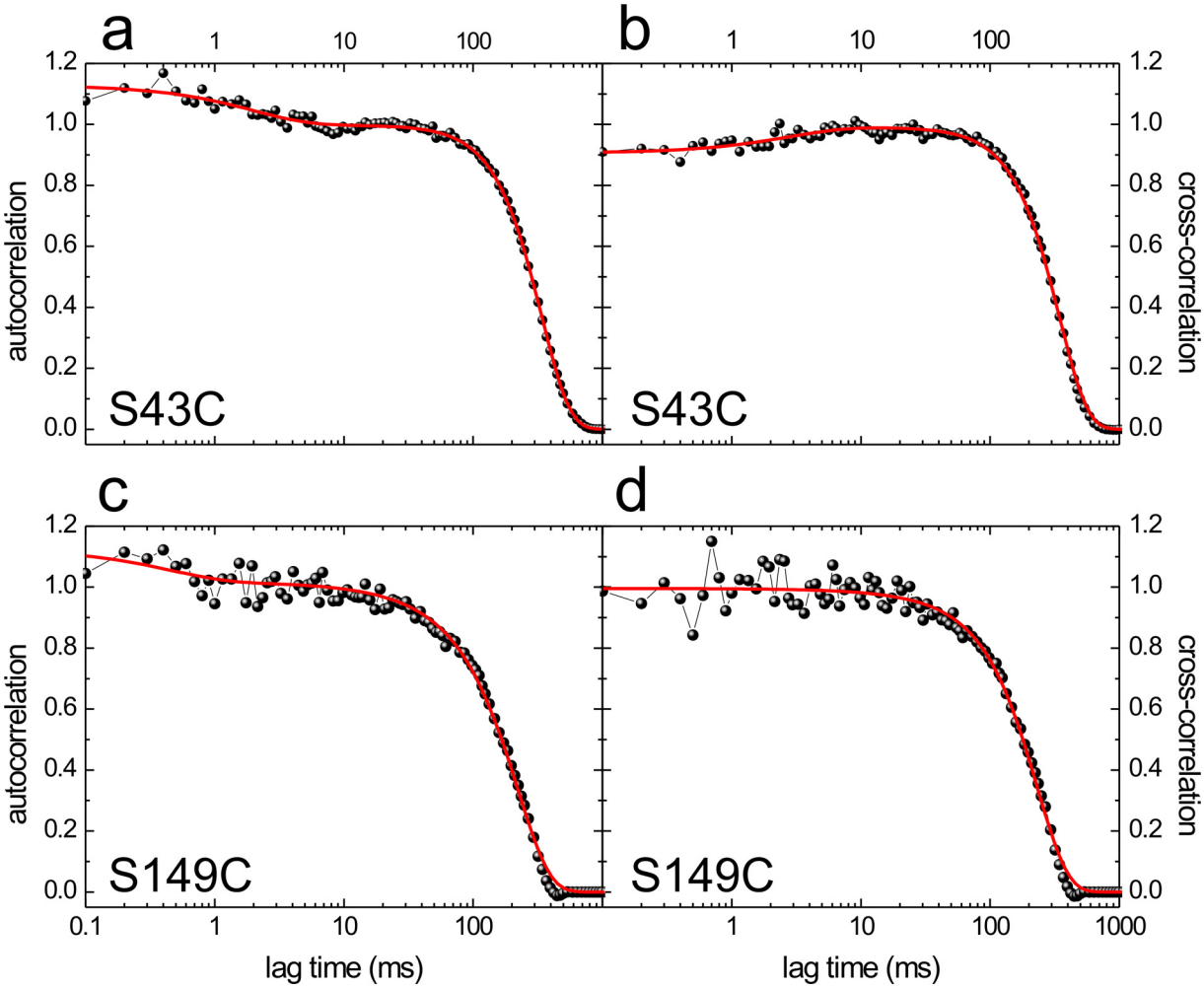

Fig. S2. Autocorrelation and cross-correlation of fluorescence intensity time traces of single, donor–acceptor-labeled kinesins show millisecond intensity fluctuations due to FRET for S43C and not for S149C. ATP concentration: 2 mM. (*a*) Autocorrelation of the fluorescence intensity time trace of Fig. S1*A* (S43C). Shown is a fit (red curve) to the data with Eq. **2**, consisting of a Gaussian (transit through confocal spot) and an exponential (FRET) component. The decay of the correlation due to FRET has an amplitude of 0.13 ± 0.01 and a decay time of 1.9 ± 0.2 ms. (*b*) Cross-correlation of donor and acceptor intensity time traces of the same S43C event as in *a*. The FRET-related exponential decay has an amplitude of −0.090 ± 0.007 and a decay time of 3.8 ± 0.7 ms. (*c*) Autocorrelation of the fluorescence intensity time trace of a full S149C event. Only a small decay of the autocorrelation on the approximate millisecond timescale can be discerned (with amplitude 0.10 ± 0.03 and decay time 0.46 ± 0.19 ms). (*d*) Cross-correlation of donor and acceptor intensity time traces of the same S149C event as in *c*. No decay of the correlation is observed on the approximate millisecond timescale, indicating that the decay observed in *c* is not due to changes in FRET, but most probably due to photo-physical effects, such as blinking of the dye.

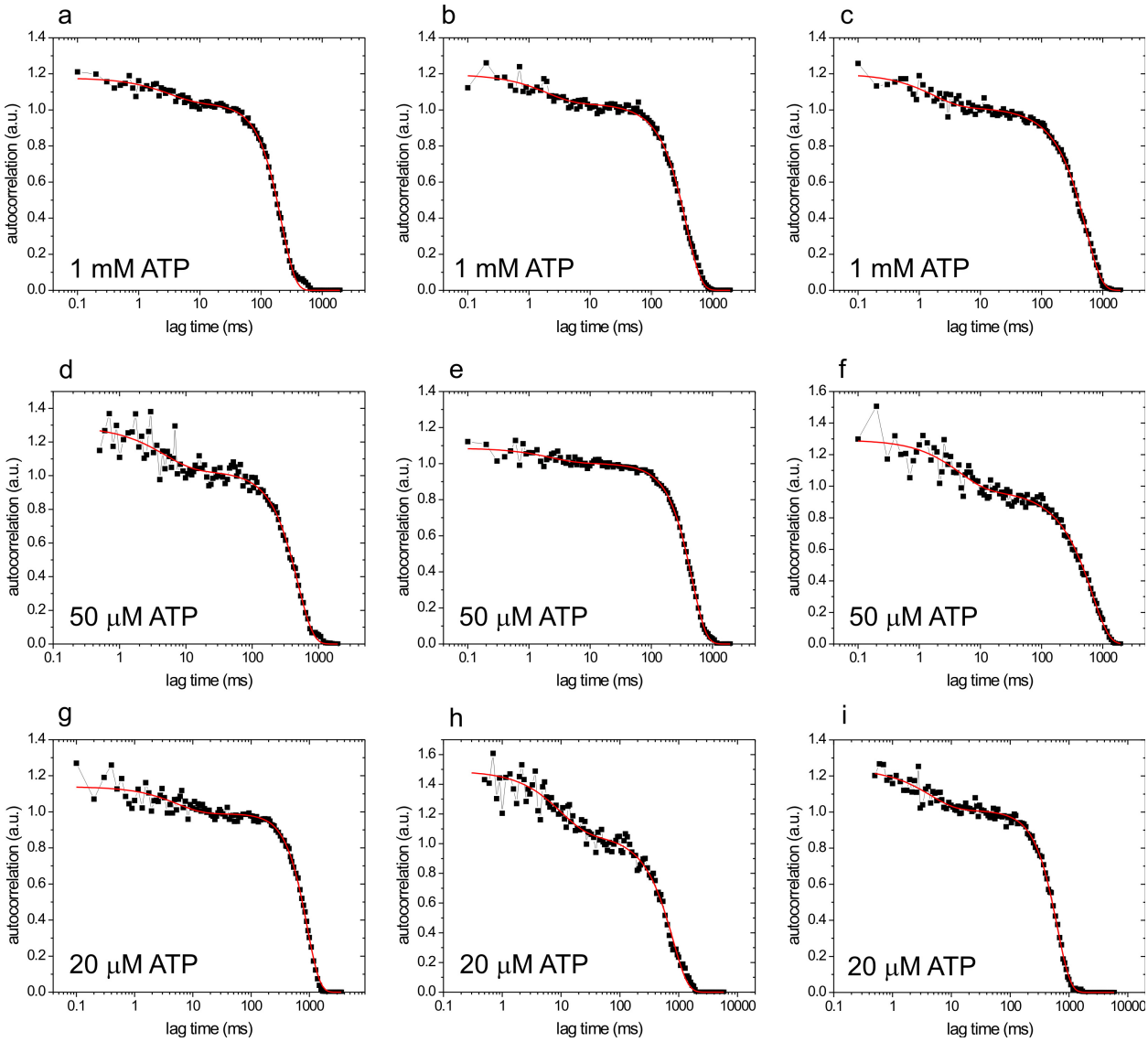

Fig. S3. Autocorrelation of the intensity time traces of single T324C events confirm that the FRET parameters alter at lower ATP concentrations. (*a–c*) Fluorescence intensity autocorrelation of three different events at 2 mM ATP concentration are shown. Fit (red, with Eq. **2**) yields amplitudes of 0.13 ± 0.01, 0.15 ± 0.01 and 0.18 ± 0.01 and decay times of 3.2 ± 0.6 ms, 1.9 ± 0.4 ms, and 1.7 ± 0.3 ms, respectively. (*d–f*) ATP concentration = 50 μM. Fit yields amplitudes of 0.25 ± 0.03, 0.08 ± 0.01, and 0.32 ± 0.03 and decay times of 4.8 ± 1.2 ms, 2.3 ± 0.6 ms, and 4.5 ± 0.8 ms, respectively. (*g–i*) ATP concentration = 20 μM. Fit yields amplitudes of 0.15 ± 0.01, 0.39 ± 0.03, and 0.42 ± 0.07 and decay times of 5.3 ± 1.1 ms, 9.7 ± 1.6 ms, and 8 ± 2 ms, respectively.

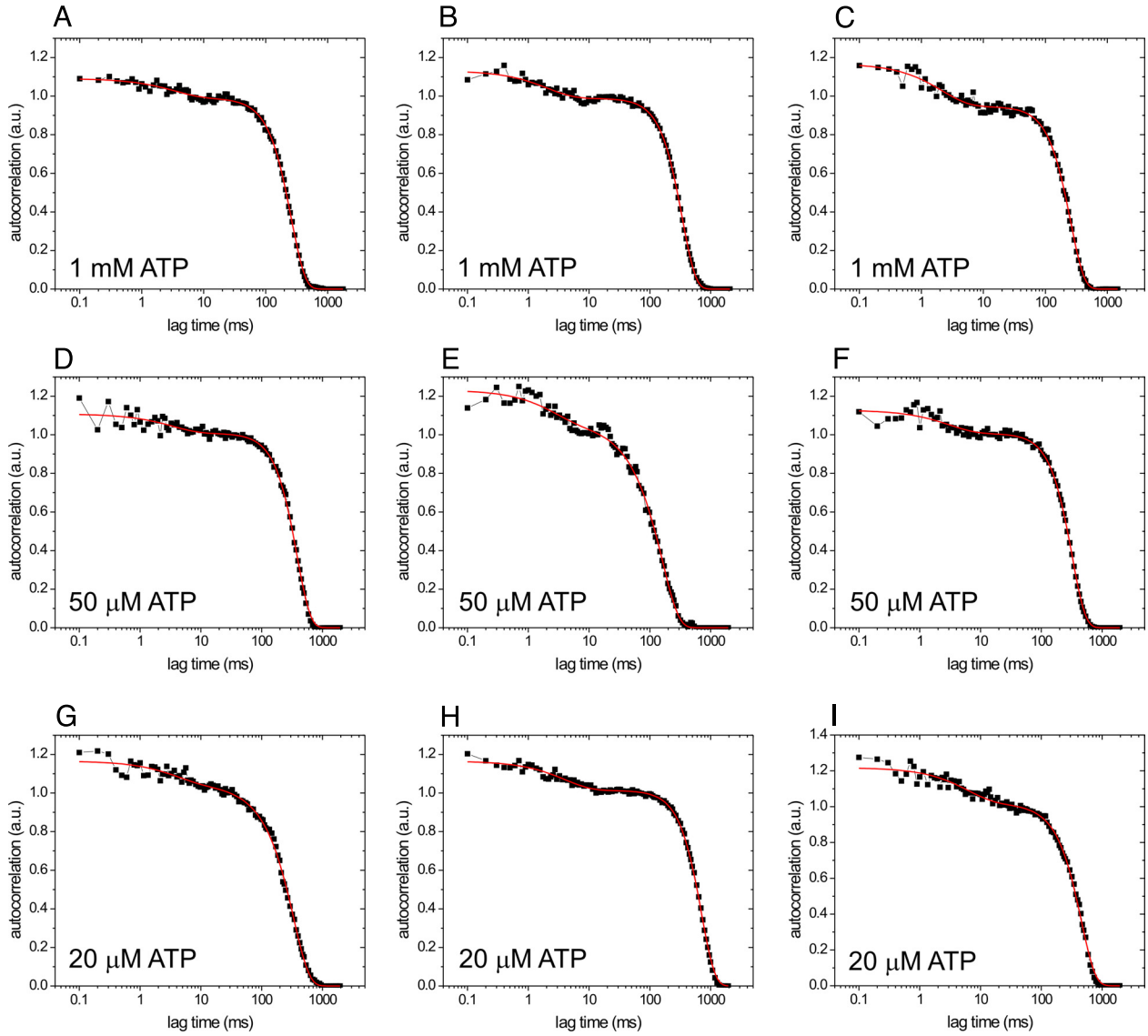

Fig. S4. Autocorrelation of the intensity time traces of single S43C events confirm that the FRET parameters alter at lower ATP concentrations. (*A–C*) Fluorescence intensity autocorrelation of three different events at 2 mM ATP concentration are shown. Fit (red, with Eq. **2**) yields amplitudes of 0.10 ± 0.01, 0.14 ± 0.01, and 0.24 ± 0.01 and decay times of 3.4 ± 0.5 ms, 2.1 ± 0.2 ms, and 2.2 ± 0.2 ms, respectively. (*D–F*) ATP concentration = 50 μM. Fit yields amplitudes of 0.10 ± 0.01, 0.15 ± 0.02, and 0.12 ± 0.01 and decay times of 3.5 ± 0.8 ms, 2.6 ± 0.6 ms, and 3.1 ± 0.5 ms, respectively. (*G–I*) ATP concentration = 20 μM. Fit yields amplitudes of 0.11 ± 0.01, 0.15 ± 0.01, and 0.19 ± 0.01 and decay times of 3.9 ± 0.9 ms, 4.1 ± 0.3 ms, and 6.1 ± 0.8 ms, respectively.

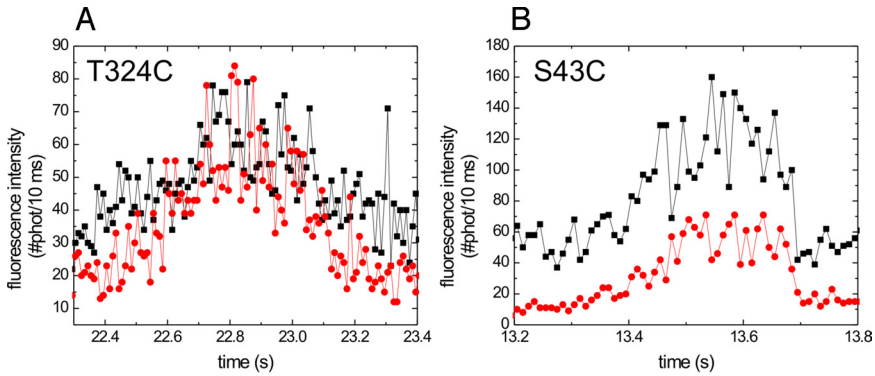

[ATP] (μM)	T324C (N = 16, 9, 5) apparent FRET efficiency	S43C (N = 19, 7, 5) apparent FRET efficiency
2000	0.43 ± 0.04	0.32 ± 0.03
50	0.50 ± 0.04	0.38 ± 0.02
20	0.63 ± 0.04	0.38 ± 0.06

F

Fig. S5. Donor (black) and acceptor (red) fluorescence intensity time traces. Traces are shown of T324C (*A*) and S43C (*B*) at 50 μM ATP. Traces are time binned over 10 ms. Apparent FRET efficiency (background corrected) of the T324C and S43C constructs at three different ATP concentrations summarized in the table (*Lower*) shows that the energy transfer increases with decreasing ATP concentration.

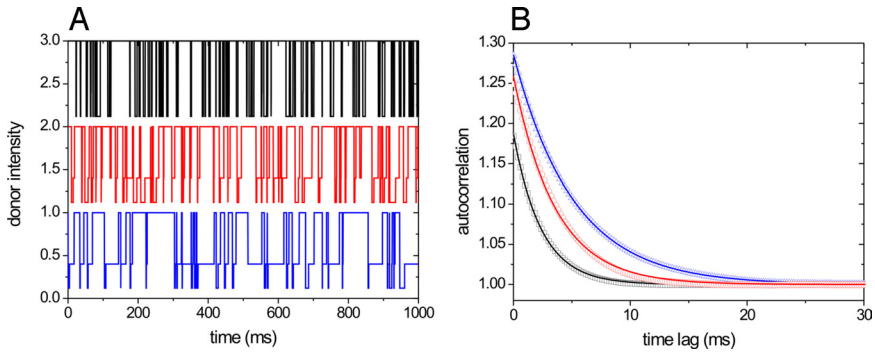

Fig. S6. Examples of simulated time traces of the T324C construct and their autocorrelations. (*A*) Time traces simulated with the three-state model at different ATP concentrations; black, red, and blue traces represent 2 mM, 50 μM, and 20 μM ATP concentration, respectively. Black and red traces have been given an offset of 2 and 1, respectively. (*B*) Autocorrelation of the simulated time traces from *A* are fitted with single-exponential-yielding amplitudes of 0.19, 0.26, and 0.27 and decay times of 2.37, 3.58, and 5.13 ms for the 2 mM, 50 μM, and 20 μM ATP concentrations, respectively.

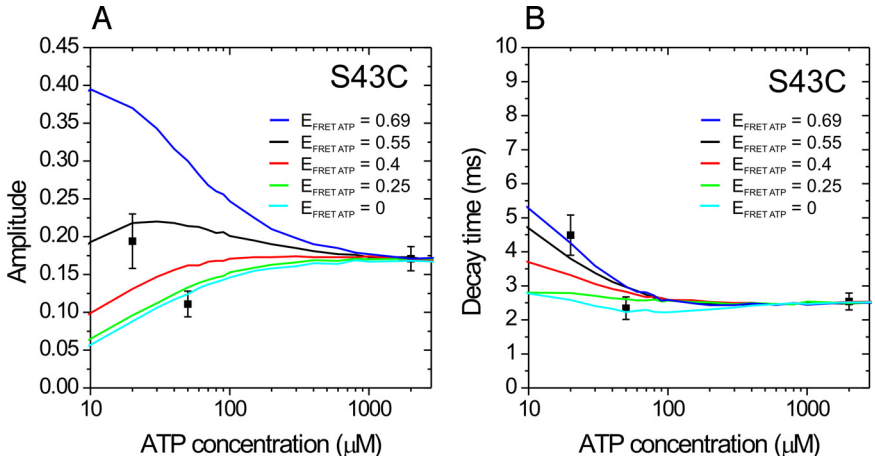

Fig. S7. Monte-Carlo simulations of FRET autocorrelation decay parameters for the S43C construct. Symbols represent parameters obtained from fitting the experimental autocorrelation curves [mean ± SEM, n = 19 (2 mM ATP), 7 (50 μM ATP), 5 (20 μM ATP)]. Simulations are shown for five different values of the FRET efficiency of the ATP-waiting state. A value of 0.40 for this parameter describes the data best. All other parameters were kept fixed ($T_{NO\ FRET}$ = 7.9 ms, $E_{NO\ FRET}$ = 0, $T_{HIGH\ FRET}$ = 3.7 ms, $E_{HIGH\ FRET}$ = 0.69, K_M = 19 μM). The simulation procedure is described in *Materials and Methods*.

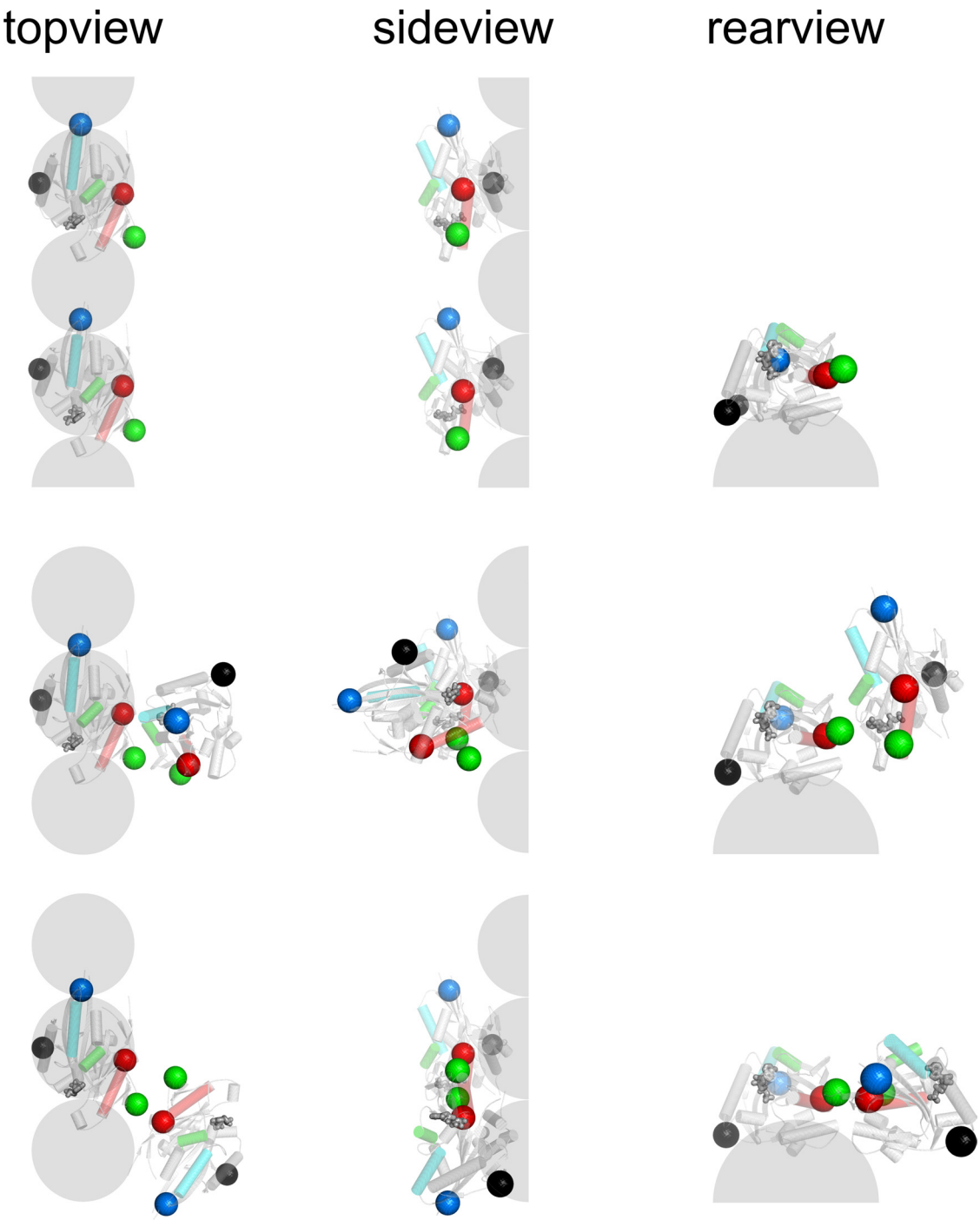

Fig. S8. Molecular model of the relative positions of both motor domains in the state in which both are MT-bound (*Topview*, three images) and two potential configurations of the high-FRET intermediate state (*Sideview* and *Rearview*, six images). These states correspond to [1] and [3] in Fig. 5, respectively. Labeling sites are indicated with spheres (43 red, 149 black, 215 blue, and 324 green). Gray (half) circles represent tubulin monomers forming a protofilament. Three helices in the motor domain are colored for clarity. The two potential intermediate configurations were obtained by applying the following restrictions: (*i*) 215–215 and 149–149 distance >6 nm. (*ii*) 324–324 and 43–43 distance <4 nm. The first possible configuration (*row 2*) has a tilted motor domain pointing away from the microtubule. Both neck linkers are in close proximity. The second possibility (*row 3*) has the unbound motor domain in the same plane as the MT-bound domain; however, it is rotated almost 180°. Models based on PDB entry 3KIN. Note that these restrictions on the location of the not-MT-bound motor domain suggest that there is no (substantial) difference between even and odd steps.

Table S1. Results of the two-state-model calculations (Eq. 3) to the fit values obtained from donor-intensity autocorrelations of T324C and S43C events at different ATP concentrations

	T324C (N = 16, 9, 5)				S43C (N = 19, 7, 5)			
[ATP], μM	T_{STEP}, ms	T_{FRET}, ms	$T_{NO\ FRET}$, ms	E_{FRET}	T_{STEP}, ms	T_{FRET}, ms	$T_{NO\ FRET}$, ms	E_{FRET}
2,000	15.0 ± 1.6	3.0 ± 0.9	12 ± 2	0.88 ± 0.12	12.1 ± 0.7	3.7 ± 0.6	7.9 ± 0.8	0.69 ± 0.06
50	22 ± 3	4.4 ± 1.1	18 ± 3	0.96 ± 0.15	13.2 ± 1.2	3.1 ± 0.7	10.0 ± 1.5	0.68 ± 0.09
20	32 ± 5	8 ± 2	25 ± 6	1.00 ± 0.19	22 ± 4	5.9 ± 1.2	16 ± 4	0.83 ± 0.11

Values are averages ± SEM of N events. Number of events (N) is given in the header of the column (for an ATP concentration 2 mM, 50 μm, and 20 μm, respectively). The lifetimes of both states are ATP dependent. T_{STEP} was obtained from Gaussian fits to the time traces, not the autocorrelation function, and was an input parameter for calculation of T_{FRET} and $T_{NO\ FRET}$, see Eq. **3**.